Covalent and electrostatic incorporation of amines into hypercrosslinked polymers for increased CO_2 selectivity

Ammar H. Alahmed,[a, b] Michael E. Briggs,*[a, b] Andrew I. Cooper,[a, b] and Dave J. Adams*[c]

Abstract: Two methods of incorporating functional groups rich in nitrogen into low cost microporous hypercrosslinked polymers (HCPs) have been evaluated and the effects on the CO_2/N_2 IAST selectivity were measured. Electrostatic incorporation of an ammonium salt into a sulfonic acid-containing HCP polymer afforded a static CO_2 uptake of 2.5 mmol g^{-1} with a CO_2/N_2 IAST selectivity of 42:1 at 1 bar and 298 K. Using column breakthrough measurements with a 15:85 CO_2/N_2 mixture at 298 K and 1 bar a selectivity of 17:1 was obtained. Varying the counter ion however, resulted in polymers with lower CO_2/N_2 selectivity values. Decoration of the parent polymer with CO_2-philic imidazole followed by electrostatic ammonium salt incorporation blocked some of the micropores reducing the selectivity which re-emphasizes the role and importance of pore width for CO_2/N_2 selectivity.

Introduction

Carbon dioxide (CO_2) scrubbing using amine solutions is currently the state-of-the-art technology for post-combustion CO_2 capture.[1,2] However, the formation of carbamates caused by the chemisorption nature of the process, coupled with the high specific heat capacity of water, results in a high parasitic energy penalty for regeneration of the scrubbing solution.[3,4] Solid adsorbents, including metal-organic frameworks (MOFs),[5–9] microporous organic polymers (MOPs),[10–13] and zeolites,[14–16] can bind CO_2 either by chemisorption[17] or by physisorption, where the physical interactions are weaker.[18] The isosteric heat of adsorption (Q_{st}) indicates how strongly CO_2 binds to the adsorbent. The Q_{st} for physisorption is typically below 40–50 kJ mol^{-1}, while values over 50 kJ mol^{-1} are usually indicative of chemisorption.[19] For porous adsorbents to compete with amine solutions, certain criteria must be met including low cost of synthesis, moderate to high surface area, high CO_2 uptake, and high CO_2/N_2 selectivity.[20]

Porous organic materials can be further subdivided into crystalline solids[21] (*e.g.*, covalent organic frameworks (COFs)[22–25] and porous organic cages[26,27]) and amorphous solids (*e.g.*, polymers of intrinsic porosity (PIMs),[28,29] conjugated microporous polymers (CMPs),[10,30] and hypercrosslinked polymers (HCPs)[31–35]). HCPs are an interesting platform because they can possess high BET surface areas[32–35] and good thermal and chemical stability while being relatively inexpensive. HCPs are formed by the extensive crosslinking of aromatic monomers, which upon solvent removal affords a strained polymer that is unable to fully collapse to a non-porous state.[11] The diverse nature of the monomers available for the synthesis of HCPs (essentially any aromatic compound that possesses multiple reactive sites for Friedel-Crafts alkylation) offers potential advantages over other classes of microporous materials such as zeolites and MOFs.[9,36–38] HCPs do not require the use of expensive catalysts in their synthesis.[31] They are synthesised by Friedel-Crafts alkylation of activated aromatics in the presence of a Lewis acid catalyst such as iron(III) chloride ($FeCl_3$) using 1,2-dichloroethane (DCE) as a solvent.[11,39,40] However, these polymerisations are known to be hindered by the presence of electron-withdrawing groups such as sulfonic acids, which deactivate the ring.[41–43] This places some limitations on the functionality that can be introduced directly into HCPs. Previously, the post-synthetic introduction of sulfonic acid groups into the porous polymer network PPN-6, followed by neutralization with ammonium hydroxide (NH_4OH), was reported to enhance CO_2–network interactions.[44,45] However, PPN-6 is synthesized by Yamamoto coupling; this requires the use of expensive catalysts and starting materials under rigorously anhydrous conditions, combined with a multi-step synthesis for the brominated monomer.[46]

Owing to their low cost, ease of synthesis, and high surface area, HCPs are attractive candidates for post-synthetic modification as a strategy to enhance their moderate CO_2 uptakes and CO_2/N_2 selectivities.[35,39] Here, we report the functionalisation of HCP-SC, formed by the self-condensation of 4,4′-bis(chloromethyl)-1,1′-biphenyl (BCMBP) (Scheme 1).[39] Post-synthetic modification of HCP-SC was achieved by stirring in chlorosulfonic acid (Cl-SO_3H) and dichloromethane (DCM), followed by heating the resulting sulfonic acid derivative (HCP-SC-SO_3H) with various amines to form the corresponding ammonium salts. The effect of varying the counter-ions on CO_2 uptake at 0.15 and 1.0 bar at 298 and 328 K was studied, as well as the effect on CO_2/N_2 selectivity. We also successfully incorporated imidazole into the HCP by treating the BCMBP monomer with imidazole prior to the crosslinking reaction to afford HCP-SC-IMI (Scheme 2).[19]

Results and Discussion

Analysis of HCP-SC analogues

Due to its ease of synthesis, low cost, and high surface area HCP-SC was chosen as a candidate for post synthetic modification with the aim of producing more CO_2-philic materials.

[a] A. H. Alahmed, Dr. M. E. Briggs, Prof. A. I. Cooper
Department of Chemistry
University of Liverpool
Crown Street, Liverpool, L69 7ZD, UK
E-mail: mebriggs@liverpool.ac.uk
[b] A. H. Alahmed, Dr. M. E. Briggs, Prof. A. I. Cooper
Materials Innovation Factory
University of Liverpool
51 Oxford Street, Liverpool, L7 3NY, UK
[c] Prof. D. J. Adams
School of Chemistry, College of Science and Engineering
University of Glasgow
Glasgow, G12 8QQ, UK
E-mail: dave.adams@glasgow.ac.uk

Supporting information for this article is given via a link at the end of the document.((Please delete this text if not appropriate))

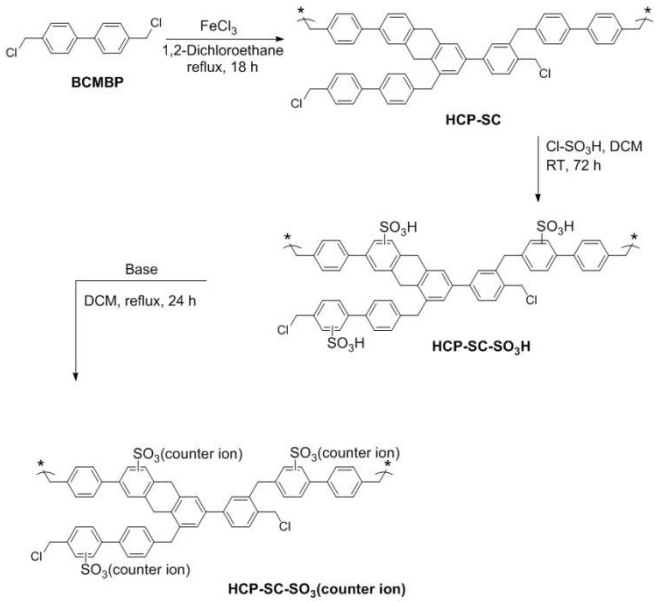

Scheme 1. Synthesis and hypothetical structure of HCP-SC analogues.

HCP-SC was prepared by refluxing BCMBP with iron(III) chloride following the route reported by Wood et al.[47] As shown in Scheme 1, post-synthetic modification of HCP-SC was achieved by stirring in Cl-SO_3H at room temperature for 3 days followed by heating the obtained sulfonic acid (HCP-SC-SO_3H) under reflux with various amines *e.g.*, NH_4OH, to form ammonium salts; in this case, HCP-SC-SO_3NH_4.

IR spectroscopy obtained for the HCP-SC network (Figure S6, Supporting Information) showed peaks at 1500 and 1600 cm^{-1} corresponding to C=C stretches from the phenylene rings in the network while the two peaks at 2800 and 3000 cm^{-1} occur due to the C–H stretching vibrations of the phenylene rings. Because some of the methyl-chloride terminal groups are not consumed during the crosslinking reaction, a peak occurring at ca. 800 cm^{-1} can be assigned to C–Cl vibrational stretch.[47] This was confirmed by oxygen flask combustion using Cheng's method, which gave a chlorine content of 2.9 wt% in the polymer. An additional vibrational stretch at ca. 3400 cm^{-1} can be assigned to adsorbed moisture in the network. The adsorbed moisture peak can also be seen in the sulfonated analogue (HCP-SC-SO_3H), where it overlaps with O–H vibrational stretch of the sulfonic acid at ca. 3400 cm^{-1}. Additional evidence of the presence of sulfonic acid groups is provided by the presence of the vibrational stretch observed at 1345 cm^{-1}, which corresponds to O=S=O.[44,48] Neutralisation of the sulfonated analogue with NH_4OH resulted in N–H vibrational stretch at ca. 3400 cm^{-1}, which also overlaps with the vibrational stretch of the entrapped water.

From CHNS microanalysis, the sulfur and nitrogen loadings in the ammonium salt analogue (HCP-SC-SO_3NH_4) were found to be 8.8 and 2.2%, respectively (Table 1); lower than the theoretical loading of 11.1 and 4.8% (Table S1, Supporting Information). The theoretical elemental loading of sulfur was calculated by assuming the incorporation of one sulfonic acid group per monomer unit,[44] while nitrogen loading was calculated by assuming full conversion of each sulfonic acid group into the ammonium salt product.[45] The calculated loading of sulfonic acid and ammonia in HCP-SC-SO_3NH_4 roughly translates to 0.7 and 0.4 units per monomer unit, respectively. It is worth noting that full conversion of the sulfonic acid into the salt was not achieved for any of the polymers, possibly because some of the sulfonic acids are inaccessible to the amine base. Also, discrepancies between calculated and theoretical CHNS microanalyses are often observed in HCPs due to adsorbed water, entrapped catalyst, or deviation for the idealised structure.[40] Similarly, the sulfonated analogue (HCP-SC-SO_3H) showed a slightly lower loading of sulfonic acid groups than expected. The calculated loading of sulfur was found to be 9.1% compared to an expected loading of 11.8%, which could be attributed to some of the unsubstituted phenylene rings being inaccessible to the Cl-SO_3H or being insufficiently activated to undergo electrophilic substitution. The calculated microanalysis of the parent polymer (HCP-SC) also showed some discrepancies in the carbon and hydrogen content, due to incomplete consumption of methyl-chloride bridges in the crosslinking reaction and physisorption of atmospheric moisture. This former was observed for related self-condensed polymers based on ortho-, meta-, and para-dichloroxylene by Wood *et al.* and was confirmed here by IR spectroscopy and combustion analysis.[47] We also attempted to react ammonia with the unreacted methyl-chlorides by stirring a suspension of HCP-SC in NH_4OH and DCM under reflux. CHN microanalysis of the isolated product indicated no nitrogen was present in the network. We therefore hypothesize that the unreacted methyl- chloride bridges are inaccessible within the polymer and are unable to undergo substitution reactions with the amines. In addition, the incorporation of the sulfonic acid functional groups

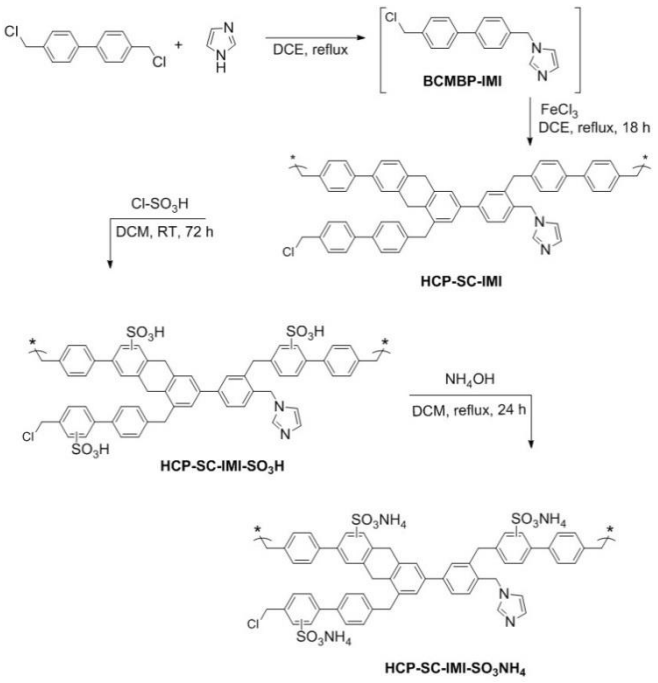

Scheme 2. Synthesis and hypothetical structure of HCP-SC-IMI analogues.

Table 1. Elemental analysis and porosity of HCP-SC, HCP-SC-SO_3H, and HCP-SC-SO_3NH_4.

Polymer[a]	CHNS microanalysis				SA_{BET}[b] [m^2 g^{-1}]	V_{Total}[c] [cm^3 g^{-1}]	CO_2 uptake[c] [mmol g^{-1}]	CO_2 uptake[d] [mmol g^{-1}]	CO_2/N_2 selectivity[e]
	%C	%H	%N	%S					
HCP-SC	89.1	5.3	-	-	1811	3.45	0.26 (0.12)	1.4 (0.8)	10:1
HCP-SC-SO_3H	57.6	4.6	-	9.1	1246	0.94	0.59 (0.23)	2.2 (1.1)	19:1
HCP-SC-SO_3NH_4	52.1	4.9	2.2	8.8	808	0.59	0.90 (0.36)	2.5 (1.4)	42:1

[a] BET surface area calculated from nitrogen isotherms at 77 K. [b] Total pore volume calculated from nitrogen adsorption isotherm in the range P/P_0=0.94–0.98. [c] CO_2 uptake at 0.15 bar/298 K (0.15 bar/328 K). [d] CO_2 total uptake at 1 bar/298 K (1 bar/328 K). [e] IAST calculated from single and dual-site Langmuir fitting isotherms in a mixture of 15/85 CO_2:N_2 at 1 bar and 298 K.

further blocks the pore network, most likely increasing their inaccessibility. The chlorine content in HCP-SC-SO_3NH_4 was found to be 2.0 wt% which confirmed that none of the methylene-chloride bridges were consumed during the sulfonation and ammonia neutralisation of HCP-SC. ICP-OES analysis of HCP-SC, HCP-SC-SO_3H, and HCP-SC-SO_3NH_4 revealed a residual Fe content of 180, 100, and 148 ppm, respectively.

The apparent Brunauer-Emmett-Teller surface area (SA_{BET}) decreased upon functionalisation from 1811 m^2 g^{-1} for the parent HCP-SC to 1246 and 808 m^2 g^{-1} for HCP-SC-SO_3H and HCP-SC-SO_3NH_4, respectively (Table 1). The parent HCP-SC showed a pronounced hysteresis in the nitrogen adsorption- desorption isotherm at 77.3 K (Figure 1), likely due to swelling, the presence of meso- and macro-pores within the network,[18,40,49] and capillary condensation.[33,50,51] We believe that these factors contribute to the high total pore volume of 3.5 cm^3 g^{-1} observed for HCP-SC (Figure 1). As expected,[44,45] the sulfonated analogue HCP-SC-SO_3H exhibited a lower surface area and pore volume than the parent polymer. However, the presence of the sulfonic acids provide stronger interaction sites for CO_2 with the polymer due to the high quadrupole moment of CO_2 and its amphoteric character.[44] As a result, the CO_2 uptake at 298 K almost doubled to 0.59 mmol g^{-1} at 0.15 bar and reached 2.2 mmol g^{-1} at 1 bar. Low pressure CO_2 uptake is more representative of power plant capture conditions, where the partial pressure of CO_2 in flue gas is approximately 0.15 bar.[52] Similarly, the CO_2/N_2 selectivity almost doubled to 19:1 at 298 K in 15/85 CO_2:N_2, due to the favourable interactions of CO_2 with sulfonic acid groups.[44]

The incorporation of ammonia into the polymer reduced the surface area and pore volume to 808 m^2 g^{-1} and 0.59 cm^3 g^{-1}, respectively. However, CO_2 uptake at 0.15 bar and 298 K increased to 0.90 mmol g^{-1} (higher than the parent acid), while the uptake at 1 bar increased to 2.5 mmol g^{-1} (Table 1). The CO_2/N_2 selectivity increased to 42:1 for HCP-SC-SO_3NH_4, which is a promising value for this class of relatively inexpensive polymer. The higher selectivity observed for HCP-SC-SO_3NH_4 compared to HCP-SC-SO_3H and HCP-SC, is due to the presence of the ammonium salt (–SO_3NH_4) and a narrowing of the micropores,

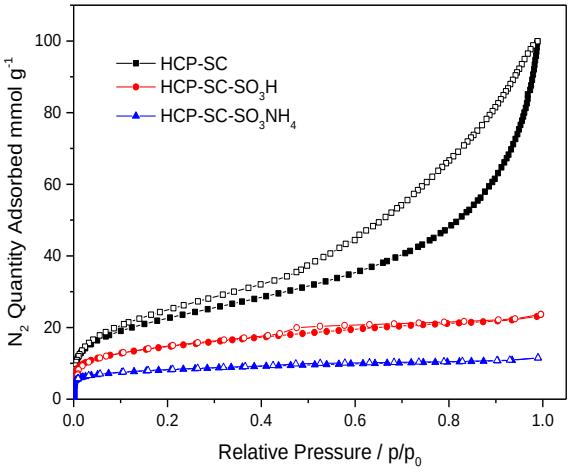

Figure 1. Adsorption-desorption isotherms for HCP-SC, HCP-SC-SO_3H and HCP- SC-SO_3NH_4 at 77.3 K. Adsorption (filled symbols), desorption (hollow symbols).

which improve the strength of the polymer-CO_2 interaction (Figure 2 & Figure S1, Supporting Information). The selectivity is similar to that reported for the more expensive nitro-rich (–NO_2) hypercrosslinked triptycene analogue (TPP-4)[53] (42.5:1 at 1 bar and 298 K in 15/85 CO_2:N_2 mixture) but lower than the copper-catalysed azo-linked polymer (ALP-7), which has a selectivity of 56:1 at 1 bar and 298 K in 10/90 CO_2:N_2 mixture.[54] The CO_2/N_2 selectivity for HCP-SC-SO_3NH_4 is significantly lower than the previously reported sulfonated PPN-6 analogue (155:1 at 1 bar and 295 K in 15/85 CO_2:N_2 mixture)[44] and its ammonium sulfonate salt (796:1 at 1 bar and 313 K in 15/85 CO_2:N_2 mixture),[45] but again we would contend that these HCP materials are much more scalable. In addition to IAST selectivity, we collected breakthrough curves for HCP-SC- SO_3NH_4. Using a binary mixture of CO_2 and N_2 in 15:85 ratio at

Table 2. Elemental analysis and porosity of the different counter ion analogues; HCP-SC-SO_3TEA, HCP-SC-SO_3ETA, HCP-SC-SO_3IMI, and HCP-SC-SO_3EN.

Polymer[a]	CHNS microanalysis				SA_{BET}[b] [$m^2\ g^{-1}$]	V_{Total}[c] [$cm^3\ g^{-1}$]	CO_2 uptake[c] [mmol g^{-1}]	CO_2 uptake[d] [mmol g^{-1}]	CO_2/N_2 selectivity[e]
	%C	%H	%N	%S					
HCP-SC-SO_3TEA	62.4	5.7	2.2	8.6	582	0.47	0.32 (0.16)	1.2 (0.79)	6:1
HCP-SC-SO_3ETA	49.8	5.1	2.8	7.3	546	0.34	0.41 (0.17)	1.5 (0.81)	8:1
HCP-SC-SO_3IMI	61.8	4.8	5.8	9.1	657	0.39	0.43 (0.18)	1.5 (0.80)	18:1
HCP-SC-SO_3EN	57.6	5.5	5.4	7.9	509	0.34	0.49 (0.22)	1.6 (0.98)	12:1

[a] BET surface area calculated from nitrogen isotherms at 77 K. [b] Total pore volume calculated from nitrogen adsorption isotherm in the range P/P_0=0.94–0.98. [c] CO_2 uptake at 0.15 bar/298 K (0.15 bar/328 K). [d] CO_2 total uptake at 1 bar/298 K (1 bar/328 K). [e] IAST calculated from single and dual-site Langmuir fitting isotherms in a mixture of 15/85 CO_2:N_2 at 1 bar and 298 K.

298 K and 1 bar with a helium purge between runs (Figure S20, Supporting Information). A total of 6 breakthrough cycles were run showing no loss in CO_2 capacity and selectivity. HCP-SC-SO_3NH_4 CO_2/N_2 selectivity was calculated to be 17:1,[55] lower than IAST value; this may be the result of slower adsorption kinetics of CO_2 into the polymer under conditions similar to flue gas streams.[56]

The Q_{st} of each of the analogues was calculated from three CO_2 uptake isotherms at 298, 318, and 328 K. The CO_2 Q_{st} for HCP-SC was around 19 kJ mol^{-1} in the zero-coverage region. This value is relatively low, as expected due to the lack of CO_2 polarizing groups within the network.[44] Incorporation of sulfonic acids into HCP-SC almost doubled the Q_{st} to ca. 37 kJ mol^{-1}, while the Q_{st} of HCP-SC-SO_3NH_4 was found to be 36 kJ mol^{-1} (Figure 3). The reported Q_{st} of the sulfonic acid of PPN-6 and its ammonium salt were ca. 30 and 40 kJ mol^{-1}, respectively,[45] similar to the values we obtained for these cheaper HCP-SC sulfonated and ammonium salt analogues.

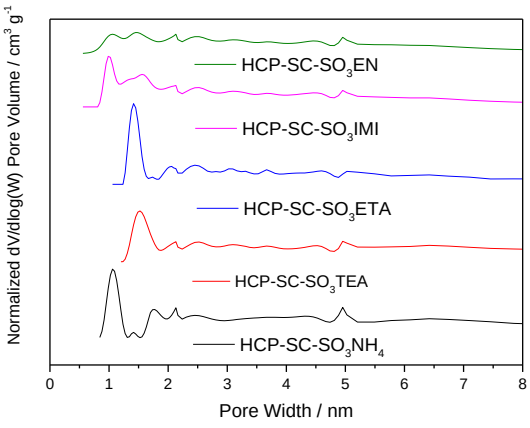

Figure 2. Pore-size distribution calculated using pillared clay model of NL-DFT method assuming cylindrical pores for HCP-SC salt analogues with various counter ions.

Analysis of different counterion analogues

In an attempt to increase the CO_2/N_2 selectivity in HCP-SC networks through derivatisation to incorporate CO_2-philic functional groups, we investigated the variation of the counter ion on CO_2 selectivity and uptake. To introduce different counterions, the sulfonic acid, HCP-SC-SO_3H, was stirred under reflux for 24 hours in a DCM solution of the specified amine- base. Four different analogues were prepared (Scheme 1) containing triethylamine (TEA), ethanolamine (ETA), imidazole (IMI), and ethylenediamine (EN) as counterions (HCP-SC-SO_3TEA, HCP-SC-SO_3ETA, HCP-SC-SO_3IMI and HCP-SC-SO_3EN, respectively).

IR spectroscopy obtained for the different analogues (Figure S7, Supporting Information) showed a trapped moisture peak at ca. 3400 cm^{-1}. The assignment of C–N stretches is difficult due to overlap with O=S=O peaks in the region of 1000–1350 cm^{-1} and perhaps the sp^3 C–H bend in the region of ca. 1300 to 1400 cm^{-1}. As stated previously, theoretical CHNS microanalysis was calculated assuming full conversion of the sulfonic acid to the ammonium salt. The nitrogen loading varies across the analogues, with discrepancies observed between the calculated and theoretical values. The lowest nitrogen loading was observed in HCP-SC-SO_3TEA and HCP-SC-SO_3ETA of 2.2 and 2.8%, respectively, which indicated that conversion of the sulfonic acids to the desired salt was not fully achieved (Table S1, Supporting Information). HCP-SC-SO_3EN and HCP-SC-SO_3IMI analogues showed the highest loading of nitrogen of 5.4 and 5.8%

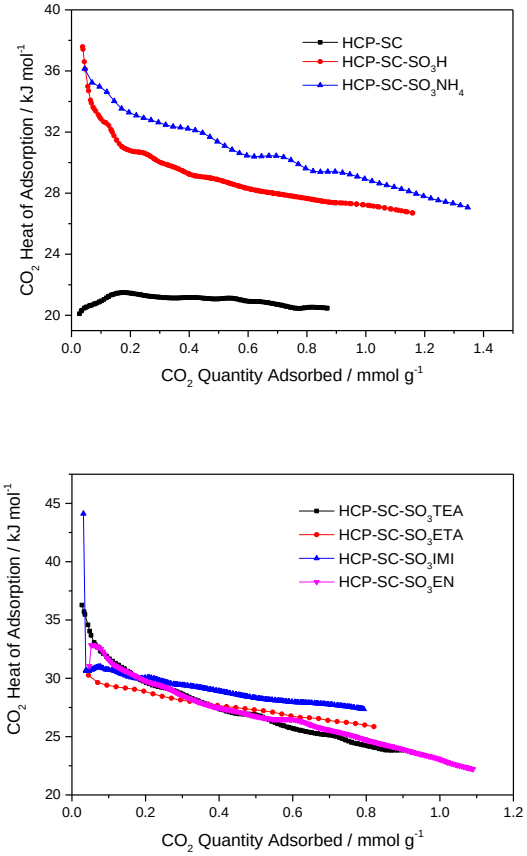

Figure 3. CO_2 isosteric heat of adsorption calculated from three temperatures (298, 318, and 328 K). Top: HCP-SC, HCP-SO_3H and HCP-SC-SO_3NH_4. Bottom: different counterion analogues.

mainly due to their higher nitrogen content when compared to triethylamine and ethanolamine.

The SA_{BET} of these salts decreased with respect to the parent acid polymer to values of between 509 and 657 m^2 g^{-1} (Tables 1 and 2). We anticipated that the various counterions might interact differently with CO_2, thus resulting in different CO_2/N_2 selectivity values.[57] For instance, the delocalized positive charge over imidazolium[57] might result in weaker interactions with CO_2 when compared to HCP-SC-SO_3EN.[58]

The highest CO_2/N_2 selectivity among these analogues was 18:1, as obtained for the imidazolium salt, HCP-SC-SO_3IMI. We ascribe this to a combination of the CO_2–imidazolium salt interactions and the narrower pores present in the imidazolium analogue compared to the other three alkylammonium analogues (Figure 2). However, the selectivity for HCP-SC-SO_3IMI is lower than that observed for the ammonium salt, above, which has a CO_2/N_2 selectivity of 42:1; this is probably because of its high localized positive charge density, which results in stronger CO_2 interactions.[57,59] As a result, the uptake of CO_2 in the low pressure region was measured to be 0.90 vs 0.43 mmol g^{-1} for the ammonium and imidazolium salts, respectively. Similarly, the total uptake of CO_2 at 1 bar was higher for the ammonium salt as a result of its higher surface area of 808 m^2 g^{-1} compared to 657 m^2 g^{-1} for the imidazolium salt (Tables 1 and 2). Hence, alkylated amines did not provide a selectivity or CO_2 capacity benefit with respect to the ammonium salt, HCP-SC-SO_3NH_4.

The presence of nitrogen in the polymer increases the number of preferential CO_2 binding sites.[60–63] This can be seen in the case of the ethylenediamine-containing salt. Despite HCP-SC-SO_3EN having a pore volume of only 0.34 cm^3 g^{-1} and a SA_{BET} of 509 m^2 g^{-1}, its CO_2/N_2 selectivity was calculated to be 12:1. Although the HCP-SC-SO_3ETA analogue has a similar pore volume of 0.34 cm^3 g^{-1} and a slightly higher SA_{BET} of 546 m^2 g^{-1}, its CO_2/N_2 selectivity decreased to 8:1. We ascribe the drop in selectivity to the blocking of the narrower micropores (<1.0 nm) in HCP-SC-SO_3ETA in addition to its lower nitrogen content compared to HCP-SC-SO_3EN (Figure 2).[38,64,65] CO_2/N_2 selectivity was lowest for HCP-SC-SO_3TEA, where blocking of the narrower micropores and steric hindrance around the nitrogen lowered its selectivity to 6:1. Although nitrogen loading provides stronger binding sites for CO_2, pore width also plays an important role.[64]

Varying the counter ions also has an impact on Q_{st} values and how strongly the CO_2 interacts with the polymers. The imidazolium salt showed the highest Q_{st} of 45 kJ mol^{-1} in the zero-coverage region, which is higher than the ammonium salt, HCP-SC-SO_3NH_4 (Figure 3). Ethylenediamine and ethanolamine analogues showed Q_{st} of 31 and 32 kJ mol^{-1}, respectively in the zero-coverage region while the triethylamine analogue was slightly higher with a value around 36 kJ mol^{-1} in the zero-coverage region. The Q_{st} values of the different salts all fall within physisorption range.[19]

Analysis of HCP-SC-IMI analogues

Full conversion of the sulfonic acid to the salt was not achieved for any of these polymers, most likely due to some of the sulfonic acids being inaccessible to the amine bases. We therefore decided to covalently attach imidazole to BCMBP prior to the crosslinking reaction, and to study the effect on the CO_2 uptake and CO_2/N_2 selectivity. The BCMBP monomer was reacted with imidazole (6:1 ratio) in DCE under reflux and nitrogen. The crosslinking reaction was then induced by the addition of $FeCl_3$ and heating under reflux to yield HCP-SC-IMI (Scheme 2). Similar to HCP-SC, HCP-SC-IMI was also derivatised to yield the corresponding sulfonated and ammonium salt analogues; HCP-SC-IMI-SO_3H and HCP-SC-IMI-SO_3NH_4.

^{1}H NMR spectra of BCMBP-IMI in the reaction mixture (Figure S19, Supporting Information) confirmed the attachment of imidazole to BCMBP through the appearance of three singlet peaks between 5.48–5.54 ppm, suggesting the presence of three new methylene environments. These correspond to methylene protons adjacent to an imidazole, which is formed by the displacement of the chloride at one or both ends of the BCMBP. It is also possible for an imidazole to act as a bridge between two molecules of BCMBP. Protonation of any mono- substituted imidazole by the HCl generated in the reaction is also a possibility and might explain the presence of peaks between 9.11 and 9.57 ppm in the ^{1}H NMR. The peak at 4.8 ppm corresponds to the methyl-chloride; since imidazole was reacted in limitation, the

Table 3. Elemental analysis and porosity of HCP-SC-IMI, HCP-SC-IMI-SO_3H, and HCP-SC-IMI-SO_3NH_4.

Polymer[a]	CHNS microanalysis				SA_{BET}[b] [$m^2\ g^{-1}$]	V_{Total}[c] [$cm^3\ g^{-1}$]	CO_2 uptake[c] [mmol g^{-1}]	CO_2 uptake[d] [mmol g^{-1}]	CO_2/N_2 selectivity[e]
	%C	%H	%N	%S					
HCP-SC	84.0	5.4	1.5	-	1049	0.95	0.36 (0.11)	1.7 (0.8)	14:1
HCP-SC-IMI-SO_3H	58.2	4.6	0.9	9.5	745	0.72	0.54 (0.24)	1.7 (1.1)	29:1
HCP-SC-IMI-SO_3NH_4	53.9	4.8	3.0	8.7	642	0.54	0.79 (0.35)	2.1 (1.3)	30:1

[a] BET surface area calculated from nitrogen isotherms at 77 K. [b] Total pore volume calculated from nitrogen adsorption isotherm in the range P/P_0=0.94–0.98. [c] CO_2 uptake at 0.15 bar/298 K (0.15 bar/328 K). [d] CO_2 total uptake at 1 bar/298 K (1 bar/328 K). [e] IAST calculated from single and dual-site Langmuir fitting isotherms in a mixture of 15/85 CO_2:N_2 at 1 bar and 298 K.

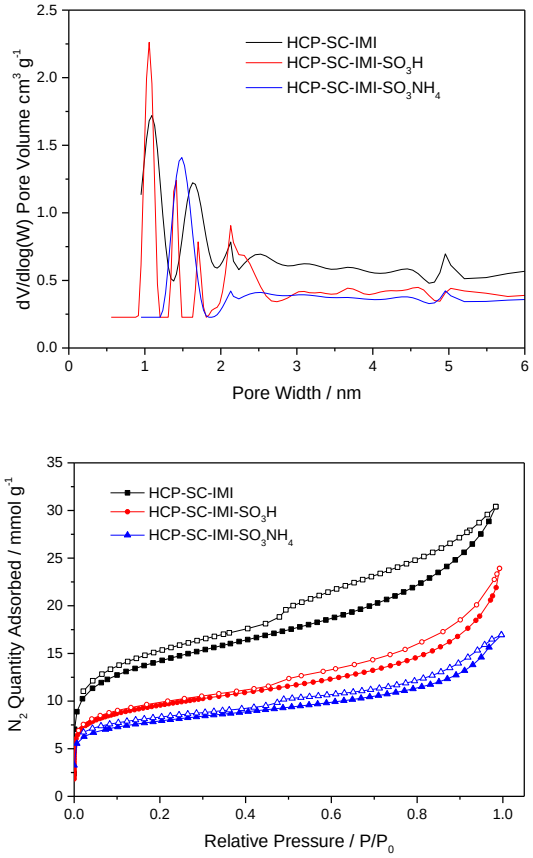

Figure 4. Top) Pore-size distribution for HCP-SC-IMI analogues calculated using pillared clay model of NL- DFT method assuming cylindrical pores. Bottom) Nitrogen isotherms of HCP-SC-IMI analogues at 77.3 K. Adsorption (filled symbols), desorption (hollow symbols).

higher intensity of this peak when compared to the methyl-imidazole resonance was anticipated. Due to the lower intensity of the methyl-imidazole in BCMBP-IMI, ^{13}C NMR signal of the methyl carbon was below the level that could be detected.

IR spectroscopy obtained for HCP-SC-IMI analogue (Figure S8, Supporting Information) showed a stronger intensity at ca. 3450 cm^{-1} compared to HCP-SC. However, the overlap of the N–H stretch with the O–H vibrational stretch makes it difficult to assign the protonated imidazole vibrational stretch. The appearance of O=S=O stretch at ca. 1250 cm^{-1} in the IR spectra of HCP-SC-IMI-SO_3H confirmed the presence of the sulfonic acid. Similar to the HCP-SC-SO_3NH_4, the assignment of N–H stretch is difficult due to overlapping with the O–H of the trapped moisture and the sulfonic acid groups (Figure S8, Supporting Information).

Due to the incorporation of the imidazole and the fewer methyl-chloride groups being available for crosslinking, the SA_{BET} and pore volume of HCP-SC-IMI decreased to 1049 $m^2\ g^{-1}$ and 0.95 $cm^3\ g^{-1}$, respectively, when compared to HCP-SC (Tables 1 and 3). The nitrogen sorption isotherm of HCP-SC-IMI at 77.3 K showed less hysteresis than for HCP-SC due to less inner-stress within the network as a result of the fewer crosslinking bridges (Figure 4).[34,66] The CO_2 uptake at 0.15 bar and 298 K, increased by around 40%, from 0.26 mmol g^{-1} in HCP-SC to 0.36 mmol g^{-1} in HCP-SC-IMI, while the uptake at 1 bar and 298 K was 1.7 mmol g^{-1} for HCP-SC-IMI compared to 1.4 mmol g^{-1} for HCP-SC under similar conditions (Tables 1 and 3). The increase in CO_2 capacity is likely due to the presence of the Lewis basic nitrogen in HCP-SC-IMI,[62,65] which would also explain the high Q_{st} of 45 kJ mol^{-1} (Figure S5, Supporting Information). The Q_{st} value falls near the chemisorption region of 50 kJ mol^{-1}, but the reversibility of CO_2 isotherms suggests that the polymer maintains a physisorption adsorption mechanism.

Encouraged by these results, we hypothesised that further post-synthetic modification of HCP-SC-IMI to introduce the ammonium salt could result in an increase in CO_2/N_2 selectivity. Sulfonation was carried out in a similar manner to the HCP-SC network (Scheme 2). HCP-SC-IMI-SO_3H had a sulfur content of 9.5% (Table 3) and a SA_{BET} of 745 $m^2\ g^{-1}$. The CO_2 uptake at 1 bar and 298 K did not change when compared to the parent polymer, but the CO_2/N_2 selectivity almost doubled to 29:1 because of an increase in CO_2 uptake at low pressure. Stirring the sulfonated analogue in ammonium hydroxide afforded HCP-SC-IMI-SO_3NH_4, which has the lowest SA_{BET} amongst HCP-SC-IMI analogues of 642 $m^2\ g^{-1}$. The CO_2 uptake at 1 bar and 298 K, however, increased to 2.1 mmol g^{-1} despite the total pore volume decreasing to 0.54 $cm^3\ g^{-1}$. The corresponding selectivity value was 30:1; lower than the 42:1 value that was obtained for HCP-SC-SO_3NH_4 both at 1 bar and 298 K in 15/85 CO_2:N_2 mixture. This loss of selectivity is attributed to the loss of some micropores in HCP-SC-IMI-SO_3NH_4 that are present in HCP-SC-SO_3NH_4 (Figures 2 and 4). This result emphasizes the important role pore size distribution plays in obtaining high CO_2/N_2 selectivity.[38,64,65]

Finally, the Q_{st} of the sulfonated analogue (HCP-SC-IMI-SO_3H) dropped to 36 kJ mol^{-1} compared to HCP-SC-IMI but the selectivity almost doubled. The ammonium salt analogue showed a slightly lower Q_{st} value of 35 kJ mol^{-1}, but due to the loss of some of the narrower micropores the CO_2/N_2 selectivity has not improved compared to the sulfonated analogue (Figure S5, Supporting Information).

Conclusions

In conclusion, we have combined two approaches—electrostatic and covalent attachment—to maximise amine loading in BCMBP-derived HCPs in an attempt to increase CO_2/N_2 selectivity. After screening a range of amines, we found that ammonium salts afforded the highest CO_2 uptakes and selectivities for HCP-SC-SO_3NH_4 and HCP-SC-IMI-SO_3NH_4, respectively. The presence of additional micropores in the HCP-SC-SO_3NH_4 afforded the highest selectivity of CO_2 over nitrogen for all the materials tested. Finding the right tradeoff between nitrogen loading and pore diameter is important to achieve high CO_2/N_2 selectivity.

Experimental Section

Materials and methods: 4,4′-Bis(chloromethyl)-1,1′-biphenyl was obtained from TCI chemicals, UK. All other reagents were purchased from Sigma-Aldrich and used as received.

Synthesis of HCP-SC: To a solution of BCMBP (2.14 g, 8.52 mmol) in anhydrous DCE (20 mL), was added $FeCl_3$ (1.38 g, 8.52 mmol) under a nitrogen atmosphere. The resulting mixture was heated under reflux for 18 hours. The brown precipitate was washed with water (50 mL), methanol (3 x 50 mL), and with diethyl ether (50 mL) followed by drying for 24 hours at 60 °C under vacuum to produce HCP-SC (yield = 1.52 g) (Scheme 1).

Derivatisation of BCMBP with imidazole: Under a nitrogen atmosphere, a solution of BCMBP (1.38 g, 5.49 mmol) and imidazole (0.06 g, 0.88 mmol) in DCE (40 mL) was heated under reflux overnight, at which time the imidazole was consumed (monitored by TLC) to produce BCMBP-IMI (Scheme 2).

Synthesis of HCP-SC-IMI: $FeCl_3$ (0.89 g, 5.49 mmol) was added to the above mixture of BCMBP-IMI then the reaction was heated under reflux overnight. After cooling, the precipitate was collected by filtration and washed with water (50 mL) and methanol (3 x 50 mL). The solid was further purified by Soxhlet extraction in methanol for 24 hours, then dried in a vacuum oven at 60 °C for 24 hours to produce HCP-SC-IMI (yield = 1.27 g) (Scheme 2).

General procedure for sulfonation of HCP-SC and HCP-SC-IMI: An ice-bath-cooled suspension of HCP-SC (200 mg) in DCM (20 mL) was stirred and allowed to swell for a few hours. To this was added Cl-SO_3H (6 mL, 90 mmol) drop-wise. The resulting mixture was stirred at room temperature for three days then poured into ice. The solid was collected, thoroughly washed with methanol and water, then dried at 60 °C under vacuum to produce HCP-SC-SO_3H (yield = 262 mg) (Scheme 1). The same procedure was followed using HCP-SC-IMI to produce HCP-SC-IMI-SO_3H (yield = 278 mg) (Scheme 2).

General procedure for ammonium salt formation with HCP-SC-SO_3H and HCP-SC-IMI-SO_3H: A suspension of HCP-SC-SO_3H (150 mg) in 10 mL DCM was allowed to swell for a few hours. NH_4OH solution (20 mL) was added and the mixture was heated under reflux overnight. The solid was collected, thoroughly washed with water and methanol, and then dried at 60 °C under vacuum to produce HCP-SC-SO_3NH_4 (yield = 150 mg) (Scheme 1). The same procedure was followed using HCP-SC-IMI-SO_3H to produce HCP-SC-IMI-SO_3NH_4 (yield = 195 mg) (Scheme 2).

Salt formation with HCP-SC-SO_3H and TEA, ETA, IMI, and EN: (a) Synthesis of HCP-SC-SO_3TEA: An ice-bath-cooled mixture of HCP-SC-SO_3H (150 mg) in DCM (10 mL) was allowed to swell for few hours. To this, was added trimethylamine (TEA) (20 mL) and the mixture was heated under nitrogen and reflux overnight. The solid was collected, thoroughly washed with water and methanol, and then dried at 60 °C to produce HCP-SC-SO_3TEA (yield = 122 mg). (b) Synthesis of HCP-SC-SO_3ETA: As for (a), but ethanolamine (ETA) was used instead of triethylamine (TEA) to afford HCP-SC-SO_3ETA (yield = 204 mg). (c) Synthesis of HCP-SC-SO_3IMI: An ice-bath-cooled mixture of HCP-SC-SO_3H (150 mg) in DCM (20 mL) was allowed to swell for few hours. To this, was added imidazole (IMI) (2.0 g, 0.03 mol) and the mixture was heated under reflux overnight. The solid was collected, thoroughly washed with water and methanol, and

then dried at 60 °C under vacuum to produce HCP-SC-SO_3IMI (yield = 195 mg). (d) Synthesis of HCP-SC-SO_3EN: An ice-bath-cooled mixture of HCP-SC-SO_3H (100 mg) in DCM (10 mL) was allowed to swell for few hours. To this, was added ethylenediamine (EN) (10 mL) and the mixture was heated under reflux overnight. The solid was collected, thoroughly washed with water and methanol, and then dried at 60 °C under vacuum for 24 hours to produce HCP-SC-SO_3EN (yield = 112 mg).

Fourier transform infrared (FTIR): IR spectra for HCP analogues were collected on a Bruker Tensor 27 using KBr disks.

Elemental analysis: CHN elemental analysis was carried out using a Thermo FlashEA 1112 Elemental Analyser and CHNS elemental analysis was carried out using an Elementar vario MICRO cube.

nuclear magnetic resonance (^{1}H NMR):. Solution ^{1}H NMR was carried out on a Bruker 400MHz Advance spectrometer.

Gas sorption. Nitrogen adsorption and desorption isotherms of the HCP analogues were collected at 77.3 K using an ASAP2420 volumetric adsorption analyser (Micrometrics Instrument Corporation). Brunauer-Emmett-Teller surface area (SA_{BET}) was calculated in the relative pressure (P/P_0) range of 0.05–0.25 and total pore volume (V_{Total}) was calculated at P/P_0 = ca. 0.89–0.99.

The pillared clay method of non-local density functional theory (NL-DFT) was used to determine the pore size distribution assuming cylindrical pore geometry. Carbon dioxide and nitrogen isotherms were collected up to a pressure of 1 bar on a Micromeritics ASAP2020 at 298 K for nitrogen and 298, 318, and 328 K for carbon dioxide. HCP analogues were degassed at 120 °C for 900 minutes under dynamic vacuum (10^{-5} bar) before analysis.

Scanning electron microscopy (SEM): A Hitachi S 4800 cold field emission scanning electron microscope (FE SEM) was used to collect high resolution imaging of the polymer morphology. The samples were loaded onto 15 mm Hitachi M4 aluminium stubs. Using an adhesive high purity carbon tab, the prepared HCP analogues were coated with gold nanolayer using an Emitech K550X automated sputter coater (25 mA for 2–3 minutes). Imaging was conducted using a mix of upper and lower secondary electron detectors at a working voltage of 3 kV and a working distance of 8 mm.

Thermogravemetric analysis (TGA):. TGA was carried out in aluminium pans using a Q5000IR analyser (TA instruments) with an automated vertical overhead thermobalance. The samples were heated at 20 °C min^{-1} to 600 °C under nitrogen followed by switching to air at 600 °C.

Breakthrough measurements: Hiden Iso-chema Automated Breakthrough Analyzer (ABR) was used to carry out breakthrough measurements for HCP-SC-SO_3NH_4. The measurements were run at 1 bar in a 15:85 CO_2/N_2 mixture at 298 K and a total flow rate of 8 mL min^{-1}.

Chlorine analysis: The anlaysis of chlorine was performed by Exter Anlytical, UK. The polymers were combusted under oxygen where Cheng's method was used to determine chlorine content in wt%.

Inductively coupled plasma optical emission spectrometry (ICP-OES): ICP-OES analysis was performed by Exter Anlytical, UK, using a Thermo iCap 7000; samples were digested with nitric acid and hydrogen peroxide in a microwave prior to analysis.

Acknowledgements

The authors would like to thank Saudi Aramco for funding. We thank Dr Tom Mitra at the University of Liverpool for collecting the SEM images.

Keywords: Hypercrosslinked polymers • CO_2 capture • microporous materials• increased selectivity • cost efficiency

References

[1] G. T. Rochelle, *Science* **2009**, *325*, 1652–1654.

[2] T. Lewis, M. Faubel, B. Winter, J. C. Hemminger, *Angew. Chemie Int. Ed.* **2011**, *50*, 10178–10181.

[3] J. D. Figueroa, T. Fout, S. Plasynski, H. McIlvried, R. D. Srivastava, *Int. J. Greenh. Gas Control* **2008**, *2*, 9–20.

[4] N. MacDowell, N. Florin, A. Buchard, J. Hallett, A. Galindo, G. Jackson, C. S. Adjiman, C. K. Williams, N. Shah, P. Fennell, *Energy Environ. Sci.* **2010**, *3*, 1645–1669.

[5] A. Ö. Yazaydın, A. I. Benin, S. A. Faheem, P. Jakubczak, J. J. Low, R. R. Willis, R. Q. Snurr, *Chem. Mater.* **2009**, *21*, 1425–1430.

[6] Y. Lin, Q. Yan, C. Kong, L. Chen, *Sci. Rep.* **2013**, *3*, 1859.

[7] A. M. Fracaroli, H. Furukawa, M. Suzuki, M. Dodd, S. Okajima, F. Gándara, J. A. Reimer, O. M. Yaghi, *J. Am. Chem. Soc.* **2014**, *136*, 8863–8866.

[8] O. Shekhah, Y. Belmabkhout, Z. Chen, V. Guillerm, A. Cairns, K. Adil, M. Eddaoudi, *Nat Commun* **2014**, *5*, 4228.

[9] Y. Liu, Z. U. Wang, H.-C. Zhou, *Greenh. Gases Sci. Technol.* **2012**, *2*, 239–259.

[10] Y. Xu, S. Jin, H. Xu, A. Nagai, D. Jiang, *Chem. Soc. Rev.* **2013**, *42*, 8012–8031.

[11] S. Xu, Y. Luo, B. Tan, *Macromol. Rapid Commun.* **2013**, *34*, 471–484.

[12] A. A. Olajire, *J. CO2 Util.* **2017**, *17*, 137–161.

[13] S. Das, P. Heasman, T. Ben, S. Qiu, *Chem. Rev.* **2017**, *117*, 1515–1563.

[14] S. Cavenati, C. A. Grande, A. E. Rodrigues, *J. Chem. Eng. Data* **2004**, *49*, 1095–1101.

[15] D. Ko, R. Siriwardane, L. T. Biegler, *Ind. Eng. Chem. Res.* **2003**, *42*, 339–348.

[16] J. Merel, M. Clausse, F. Meunier, *Ind. Eng. Chem. Res.* **2008**, *47*, 209–215.

[17] L.-J. Li, P.-Q. Liao, C.-T. He, Y.-S. Wei, H.-L. Zhou, J.-M. Lin, X.-Y. Li, J.-P. Zhang, *J. Mater. Chem. A* **2015**, *3*, 21849–21855.

[18] R. T. Woodward, L. A. Stevens, R. Dawson, M. Vijayaraghavan, T. Hasell, I. P. Silverwood, A. V Ewing, T. Ratvijitvech, J. D. Exley, S. Y. Chong, et al., *J Am Chem Soc* **2014**, *136*, 9028–9035.

[19] H. A. Patel, J. Byun, C. T. Yavuz, *ChemSusChem* **2017**, *117*, 1515–1563.

[20] T. C. Drage, C. E. Snape, L. A. Stevens, J. Wood, J. Wang, A. I. Cooper, R. Dawson, X. Guo, C. Satterley, R. Irons, *J. Mater. Chem.* **2012**, *22*, 2815–2823.

[21] A. G. Slater, A. I. Cooper, *Science* **2015**, *348*, aaa8075.

[22] A. P. Côté, A. I. Benin, N. W. Ockwig, M. O'Keeffe, A. J. Matzger, O. M. Yaghi, *Science* **2005**, *310*, 1166–1170.

[23] P. J. Waller, F. Gándara, O. M. Yaghi, *Acc. Chem. Res.* **2015**, *48*, 3053–3063.

[24] X. Feng, X. Ding, D. Jiang, *Chem. Soc. Rev.* **2012**, *41*, 6010–6022.

[25] F. J. Uribe-Romo, C. J. Doonan, H. Furukawa, K. Oisaki, O. M. Yaghi, *J. Am. Chem. Soc.* **2011**, *133*, 11478–11481.

[26] T. Tozawa, J. T. A. Jones, S. I. Swamy, S. Jiang, D. J. Adams, S. Shakespeare, R. Clowes, D. Bradshaw, T. Hasell, S. Y. Chong, et al., *Nat. Mater.* **2009**, *8*, 973–978.

[27] G. Zhang, M. Mastalerz, *Chem. Soc. Rev.* **2014**, *43*, 1934–1947.

[28] N. B. McKeown, P. M. Budd, *Chem. Soc. Rev.* **2006**, *35*, 675–683.

[29] N. B. McKeown, P. M. Budd, K. J. Msayib, B. S. Ghanem, H. J. Kingston, C. E. Tattershall, S. Makhseed, K. J. Reynolds, D. Fritsch, *Chem. – A Eur. J.* **2005**, *11*, 2610–2620.

[30] J.-X. Jiang, F. Su, A. Trewin, C. D. Wood, N. L. Campbell, H. Niu, C. Dickinson, A. Y. Ganin, M. J. Rosseinsky, Y. Z. Khimyak, et al.,

Angew. Chemie Int. Ed. **2007**, *46*, 8574–8578.

[31] R. Dawson, A. I. Cooper, D. J. Adams, *Prog. Polym. Sci.* **2012**, *37*, 530–563.

[32] M. P. Tsyurupa, V. A. Davankov, *React. Funct. Polym.* **2002**, *53*, 193–203.

[33] M. P. Tsyurupa, V. A. Davankov, *React. Funct. Polym.* **2006**, *66*, 768–779.

[34] V. A. Davankov, M. P. Tsyurupa, *React. Polym.* **1990**, *13*, 27–42.

[35] L. Tan, B. Tan, *Chem. Soc. Rev.* **2017**, *46*, 3322–3356.

[36] R. Dawson, A. Laybourn, R. Clowes, Y. Z. Khimyak, D. J. Adams, A. I. Cooper, *Macromolecules* **2009**, *42*, 8809–8816.

[37] A. Torrisi, R. G. Bell, C. Mellot-Draznieks, *Cryst. Growth Des.* **2010**, *10*, 2839–2841.

[38] L. Zhang, K. Jiang, M. Jiang, D. Yue, Y. Wan, H. Xing, Y. Yang, Y. Cui, B. Chen, G. Qian, *Chem. Commun.* **2016**, *52*, 13568–13571.

[39] C. F. Martin, E. Stockel, R. Clowes, D. J. Adams, A. I. Cooper, J. J. Pis, F. Rubiera, C. Pevida, *J. Mater. Chem.* **2011**, *21*, 5475–5483.

[40] B. Li, R. Gong, W. Wang, X. Huang, W. Zhang, H. Li, C. Hu, B. Tan, *Macromolecules* **2011**, *44*, 2410–2414.

[41] N. O. Calloway, *Chem. Rev.* **1935**, *17*, 327–392.

[42] K. Jiang, D. Kuang, T. Fei, T. Zhang, *Sensors Actuators B Chem.* **2014**, *203*, 752–758.

[43] T. Ratvijitvech, M. Barrow, A. I. Cooper, D. J. Adams, *Polym. Chem.* **2015**, *6*, 7280–7285.

[44] W. Lu, D. Yuan, J. Sculley, D. Zhao, R. Krishna, H.-C. Zhou, *J. Am. Chem. Soc.* **2011**, *133*, 18126–18129.

[45] W. Lu, W. M. Verdegaal, J. Yu, P. B. Balbuena, H.-K. Jeong, H.-C. Zhou, *Energy Environ. Sci.* **2013**, *6*, 3559–3564.

[46] K. J. Msayib, N. B. McKeown, *J. Mater. Chem. A* **2016**, *4*, 10110–10113.

[47] C. D. Wood, B. Tan, A. Trewin, H. Niu, D. Bradshaw, M. J. Rosseinsky, Y. Z. Khimyak, N. L. Campbell, R. Kirk, E. Stöckel, et al., *Chem. Mater.* **2007**, *19*, 2034–2048.

[48] S. Bhunia, B. Banerjee, A. Bhaumik, *Chem. Commun.* **2015**, *51*, 5020–5023.

[49] C. F. Martin, E. Stockel, R. Clowes, D. J. Adams, A. I. Cooper, J. J. Pis, F. Rubiera, C. Pevida, *J. Mater. Chem.* **2011**, *21*, 5475–5483.

[50] D.-P. Liu, Q. Chen, Y.-C. Zhao, L.-M. Zhang, A.-D. Qi, B.-H. Han, *ACS Macro Lett.* **2013**, *2*, 522–526.

[51] L. Lu, S. Wang, E. A. Müller, W. Cao, Y. Zhu, X. Lu, G. Jackson, *Fluid Phase Equilib.* **2014**, *362*, 227–234.

[52] D. M. D'Alessandro, B. Smit, J. R. Long, *Angew. Chemie Int. Ed.* **2010**, *49*, 6058–6082.

[53] Y. He, X. Zhu, Y. Li, C. Peng, J. Hu, H. Liu, *Microporous Mesoporous Mater.* **2015**, *214*, 181–187.

[54] P. Arab, E. Parrish, T. Islamoglu, H. M. El-Kaderi, *J. Mater. Chem. A* **2015**, *3*, 20586–20594.

[55] J. Liu, J. Tian, P. K. Thallapally, B. P. McGrail, *J. Phys. Chem. C* **2012**, *116*, 9575–9581.

[56] P.-Q. Liao, X.-W. Chen, S.-Y. Liu, X.-Y. Li, Y.-T. Xu, M. Tang, Z. Rui, H. Ji, J.-P. Zhang, X.-M. Chen, *Chem. Sci.* **2016**, *7*, 6528–6533.

[57] E. I. Privalova, E. Karjalainen, M. Nurmi, P. Mäki-Arvela, K. Eränen, H. Tenhu, D. Y. Murzin, J.-P. Mikkola, *ChemSusChem* **2013**, *6*, 1500–1509.

[58] W. R. Lee, S. Y. Hwang, D. W. Ryu, K. S. Lim, S. S. Han, D. Moon, J. Choi, C. S. Hong, *Energy Environ. Sci.* **2014**, *7*, 744–751.

[59] J. Tang, H. Tang, W. Sun, H. Plancher, M. Radosz, Y. Shen, *Chem. Commun.* **2005**, *0*, 3325–3327.

[60] T. M. McDonald, W. R. Lee, J. A. Mason, B. M. Wiers, C. S. Hong, J. R. Long, *J. Am. Chem. Soc.* **2012**, *134*, 7056–7065.

[61] S. Choi, T. Watanabe, T.-H. Bae, D. S. Sholl, C. W. Jones, *J. Phys. Chem. Lett.* **2012**, *3*, 1136–1141.

[62] X. Su, L. Bromberg, V. Martis, F. Simeon, A. Huq, T. A. Hatton, *ACS Appl. Mater. Interfaces* **2017**, *9*, 11299–11306.

[63] Y. Lin, Q. Yan, C. Kong, L. Chen, *Sci. Rep.* **2013**, *3*, 1859.

[64] A. K. Sekizkardes, J. T. Culp, T. Islamoglu, A. Marti, D. Hopkinson, C. Myers, H. M. El-Kaderi, H. B. Nulwala, *Chem. Commun.* **2015**, *51*, 13393–13396.

[65] B. Adeniran, R. Mokaya, *Chem. Mater.* **2016**, *28*, 994–1001.

[66] C. Wilson, M. J. Main, N. J. Cooper, M. E. Briggs, A. I. Cooper, D. J. Adams, *Polym. Chem.* **2017**, *8*, 1914–1922.

[67] A. K. Sekizkardes, S. Altarawneh, Z. Kahveci, T. İslamoğlu, H. M. El-Kaderi, *Macromolecules* **2014**, *47*, 8328–8334.